Chemical Science

ROYAL SOCIETY OF CHEMISTRY

EDGE ARTICLE

View Article Online
View Journal | View Issue

Cite this: *Chem. Sci.*, 2023, **14**, 7237

All publication charges for this article have been paid for by the Royal Society of Chemistry

Received 19th March 2023
Accepted 25th May 2023

DOI: 10.1039/d3sc01441j

rsc.li/chemical-science

Long-range hydrogen-bond relay catalyses the excited-state proton transfer reaction†

Kai-Hsin Chang,‡[a] Yu-Chiang Peng,‡[a] Kuan-Hsuan Su,‡[b] Yi-Hsien Lin,[b] Jiun-Chi Liu,[a] Ying-Hsuan Liu,[a] Chao-Hsien Hsu,[a] Hsiao-Ching Yang *[b] and Pi-Tai Chou *[a]

Solvent (*e.g.*, water)-catalyzed proton transfer (SCPT) *via* the relay of hydrogen (H)-bonds plays a key role in proton migration. In this study, a new class of 1*H*-pyrrolo[3,2-*g*]quinolines (**PyrQs**) and their derivatives were synthesized, with sufficient separation of the pyrrolic proton donating and pyridinic proton accepting sites to probe excited-state SCPT. There was dual fluorescence for all **PyrQs** in methanol, *i.e.*, normal (**PyrQ**) and tautomer 8*H*-pyrrolo[3,2-*g*]quinoline (**8H-PyrQ**) emissions. The fluorescence dynamics unveiled a precursor (**PyrQ**) and successor (**8H-PyrQ**) relationship and the correlation of an increasing overall excited-state SCPT rate (k_{SCPT}) upon increasing the N(8)-site basicity. k_{SCPT} can be expressed by the coupling reaction $k_{SCPT} = K_{eq} \times k_{PT}$, where k_{PT} denotes the intrinsic proton tunneling rate in the relay and K_{eq} denotes the pre-equilibrium between randomly and cyclically H-bonded solvated **PyrQs**. Molecular dynamics (MD) simulation defined the cyclic **PyrQs** and analyzed the H-bond and molecular arrangement over time, which showed the cyclic **PyrQs** incorporating ≧3 methanol molecules. These cyclic H-bonded **PyrQs** are endowed with a relay-like proton transfer rate, k_{PT}. MD simulation estimated an upper-limited K_{eq} value of 0.02–0.03 for all studied **PyrQs**. When there was little change in K_{eq}, the distinct k_{SCPT} values for **PyrQs** were at different k_{PT} values, which increased as the N(8) basicity increased, which was induced by the C(3)-substituent. k_{SCPT} was subject to a deuterium isotope effect, where the k_{SCPT} of 1.35×10^{10} s^{-1} for **PyrQ-D** in CH_3OD was 1.68 times slower than that (2.27×10^{10} s^{-1}) of **PyrQ** in CH_3OH. MD simulation provided a similar K_{eq} for **PyrQ** and **PyrQ-D**, leading to different proton tunneling rates (k_{PT}) between **PyrQ** and **PyrQ-D**.

Introduction

The transfer of protons *via* a relay of solvent molecules has long been proposed as a Grotthuss mechanism,[1–3] where the excess protons diffuse through the hydrogen bond (H-bond) network of water molecules or other hydrogen-bonded liquids through the formation and rupture of the covalent bonds around neighbouring solvent molecules. This mechanism, also known as proton-hopping or a proton-jump, may ubiquitously exist in bio-systems,[4] although the proof is somewhat elusive. Chemically, this can be probed by the solvent-catalyzed proton transfer (SCPT) reaction[5] of the designated chromophore in the excited state triggered by light excitation, where the proton-transferred isomer exhibits a distinct emission from that of the normal species prior to proton transfer. The ratiometric emission and the corresponding relaxation dynamics serve as a signal transduction for the mechanism study.[6]

Pertinent systems require core chromophores with proton donor and acceptor sites that possess sufficient distance between them such that intramolecular H-bond formation does not exist. As a result, if the designated molecule undergoes excited-state proton transfer in solution, in theory, either aggregate-catalyzed proton transfer or SCPT must be operative. In this regard, one of the prototypical systems is ascribed to 1*H*-pyrrolo[2,3-*b*]pyridine, or the more common name of 7-azaindole (**7AI**, see Scheme 1), which can be simply viewed as an analogous structure of the nucleobase adenine or the amino acid tryptophan.[7–10]

In the self-catalyzed proton transfer reaction, excited-state double-proton transfer takes place *via* the formation of **7AI** hydrogen-bonded (H-bonded) dimer in nonpolar solvents, resulting in the 7*H*-pyrrolo[2,3-*b*]pyridine tautomeric dimer. The associated reaction dynamics have provided valuable information regarding the role of proton-transfer tautomerization in the possible mutation of the adenine-thymine base pair.[11–13]

As for the excited-state SCPT, **7AI** has also been applied to mimic tryptophan, where excited state SCPT occurs *via* the

[a]*Department of Chemistry, National Taiwan University, Taipei, 10617 Taiwan, ROC. E-mail: chop@ntu.edu.tw*

[b]*Department of Chemistry, Fu Jen Catholic University, New Taipei City, 24205, Taiwan, ROC. E-mail: hcyang_chem@mail.fju.edu.tw*

† Electronic supplementary information (ESI) available. CCDC 2249836. For ESI and crystallographic data in CIF or other electronic format see DOI: https://doi.org/10.1039/d3sc01441j

‡ Kai-Hsin Chang, Yu-Chiang Peng, Kuan-Hsuan Su with equal contribution.

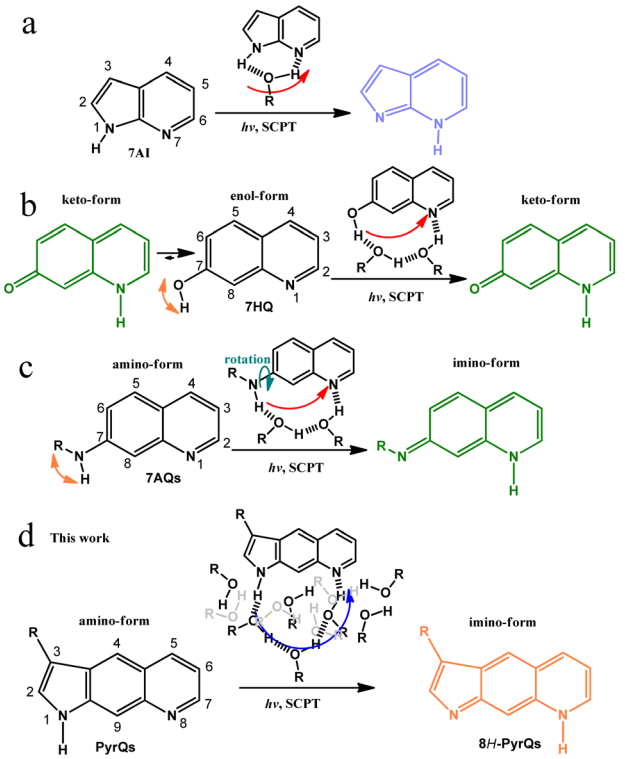

Scheme 1 (a) The well-known excited-state SCPT molecule **7AI** and the role of protic solvents in the SCPT reaction. (b) **7HQ** and its corresponding excited-state SCPT in alcohols. Note the existence of ground-state equilibrium between the enol and keto forms in alcohols.[21] (c) **7AQs** and its associated excited-state SCPT in alcohols. Note the rotation of NRH along the C(7)-N bond.[22] (d) The present work on the excited-state SCPT in **PyrQs**. In (d), both H-bonded relay alcohols required for proton transfer and bulk alcohols are presented according to the molecular dynamics (MD) simulation (see text).

formation of a 1 : 1 **7AI** : methanol cyclic H-bonded complex, resulting in the tautomer 7*H*-pyrrolo[2,3-*b*]pyridine (Scheme 1a).[8] Many studies have been performed on a number of **7AI** derivatives in protic solvents,[14,15] and the results support the mechanism of excited-state SCPT. Waluk and co-workers have studied SCPT in a number of pyrrole–pyridine systems.[16–19] Further SCPT study has been extended to another class of molecules where the 7-hydroxyquinoline enol form (**7HQ**, Scheme 1b) serves as a prototype.[20]

There is considerable distance between the proton-donating and -accepting sites of **7HQ** (*cf.* **7AI**), and the occurrence of excited-state SCPT in, *e.g.*, methanol, requires the formation of a 1 : 2 **7HQ** : methanol cyclic H-bonded complex, resulting in a keto-tautomer (Scheme 1b). However, the –OH group in **7HQ** is much more acidic than that of the pyrrolic-H group in **7AI**. Therefore, proton-transfer tautomerism also takes place for **7HQ** in the ground state, resulting in a non-negligible amount of keto-tautomer in methanol. In stronger H-bonded solvents such as water, the ground-state equilibrium between enol and keto forms is nearly 1 : 1 for **7HQ**. The co-existence of enol and keto tautomer complicates the study of excited-state SCPT.[21]

Recently, the replacement of –OH in **7HQ** by less acidic amino protons has been reported, forming 7-aminoquinoline

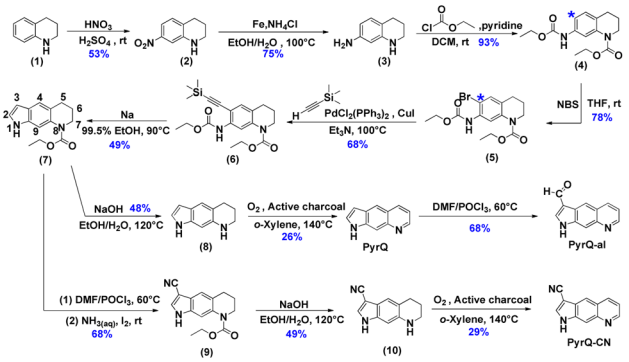

Scheme 2 The synthetic route of the studied compounds (**PyrQ**, **PyrQ-al**, and **PyrQ-CN**).

(**7AQ**, see Scheme 1c) and its derivatives, where one amino proton of $-NH_2$ can be substituted by –R, with various degrees of electron donating/withdrawing strength to fine-tune the –NRH acidity.[22] Such a configuration prevents the formation of the ground-state tautomer imino-form in methanol (Scheme 1c). However, the –NRH single bond rotation is unavoidable and results in unsymmetrical distribution of the amino proton along the C(7)-N bond (see Scheme 1c), which complicates the excited-state SCPT study. To advance in the study of long-range SCPT, it is necessary to explore a rigid system with only a single, well-defined structure in the ground state, where its proton-donating and -accepting sites are far separated at a designated distance suitable for probing fundamental insights into excited-state SCPT.

Herein, we report the strategic design and synthesis of a new class of the SCPT system by fusing the amino proton of **7AQ**, which results in the formation of pyrroloquinoline (**PyrQ**, see Scheme 1). **PyrQ** can be regarded as an extension of **7AI** by adding a fusing benzene ring between pyrrole and pyridine moieties, so that the proton donor and acceptor are far more separated than that of **7AI**. Importantly, the rigid pyrrolic ring prevents N–H rotation, and the protruding C(9)–H site (Scheme 1d) imposes steric hindrance to prevent the dimeric formation that was reported in **7AIs** under high concentration.[8] These designed strategies eliminate the aforementioned complications, which simplifies experimental and theoretical approaches (*vide infra*).

We also derivatized **PyrQ** such that the aldehyde or cyanide group can be tailored at the C(3)-position in an aim to probe the structure-SCPT relationship. The synthetic route of these **PyrQs** involves multiple steps and is non-trivial (see Scheme 2). Comprehensive spectroscopy and dynamics, together with computation in quantum mechanics and molecular dynamics (MD) approaches, were carried out to elucidate the mechanism of long-range H-bonded relay SCPT. Details are elaborated in the following sections.

Results and discussion

The details for the synthetic routes for 1*H*-pyrrolo[3,2-*g*]quinolone (**PyrQ**), 1H-pyrrolo[3,2-*g*]quinoline-3-carbaldehyde (**PyrQ-**

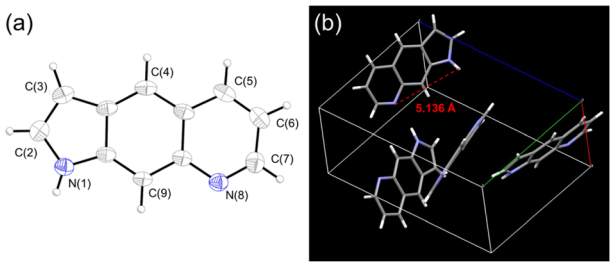

Fig. 1 (a) The molecular structure of **PyrQ** drawn with a 50% probability for a thermal ellipsoid. (b) The distance between the N(1) and N(8) atoms was calculated to be 5.136 Å.

al), and 1*H*-pyrrolo[3,2-*g*]quinoline-3-carbonitrile (**PyrQ-CN**) are depicted in Scheme 2. The details for synthesis, purification, identification, and characterization are provided in the experimental section of the ESI.† In brief, nitration of 1,2,3,4-tetrahydroquinoline (**1**) followed by reduction of $-NO_2$ yielded compound **3**.[23,24] The N–H site was then protected as carbamate by the $-COOCH_2CH_3$ group and transferred into compound **4**. The C(*)-position (see Scheme 2) of compound **4** was brominated, followed by reaction with ethynyltrimethylsilane under a palladium and copper co-catalyst, *i.e.*, the Sonogashira coupling, to obtain compound **6**.[25] A subsequent cyclization reaction transformed **6** into compound **7**, which then underwent oxidization with O_2/active charcoal to yield **PyrQ** in satisfactory yield (48%).[26]

For further derivatization, **PyrQ** was converted to **PyrQ-al** *via* the Vilsmeier–Haack reaction.[27] Also, the C(3)–H hydrogen of compound **7** was substituted with a cyano group, yielding nitrile **9** *via* one-pot transformation of electron-rich aromatics into the aromatic nitriles using the Vilsmeier–Haack reaction. Then, **9** was deprotected into **10**, but was unstable and required immediate oxidization with O_2/active charcoal to yield **PyrQ-CN**. The details regarding **PyrQ**, **PyrQ-al**, and **PyrQ-CN** characterization are elaborated in the ESI.†

The X-ray diffraction pattern of **PyrQ** is depicted in Fig. 1, and shows a fully planar configuration. Different from **7AQs** (see Scheme 1c), which have been found to have *cis*- and *trans*-forms relative to the NR-H orientation along the C–N bond,[22] there is only one configuration for **PyrQ** because of the fused pyrrolic nitrogen. The distance between the proton donor site N(1) and proton acceptor site N(8) is as far as 5.14 Å, which is significantly longer than that of 4.84 Å for **7AQ**.[22] Because of this long distance, the intrinsic intramolecular proton transfer is not feasible. Instead, in solution, if excited-state SCPT occurs, **PyrQ** requires a long-range, multiple solvent H-bond relay to bridge the proton donor and acceptor sites, which virtually act as a conduit to assist the proton transfer reaction. We also made great efforts to grow the crystal of other **PyrQs** but unfortunately failed, possibly because of hindrance by the C(3)-substitution.

Photophysical properties

Fig. 2 shows the absorption and emission spectra of **PyrQ**, **PyrQ-al**, and **PyrQ-CN**. In a non-polar aprotic solvent such as cyclohexane, **PyrQ** reveals the vibronic structured absorption spectrum with the lowest-lying absorption peak (0–0) at 370 nm. In a protic solvent such as methanol, however, the absorption of **PyrQ** significantly changes such that the lowest-lying band becomes structureless, broad, and slightly redshifted to 380 nm *versus* that in an aprotic solvent such as cyclohexane (*cf.* Fig. 2a and b). Similarly, a significant difference in absorption spectra was observed for **PyrQ-al** and **PyrQ-CN** in cyclohexane and methanol (Fig. 2). The results clearly imply that all studied **PyrQs** undergo H-bond formation with methanol solvents in the

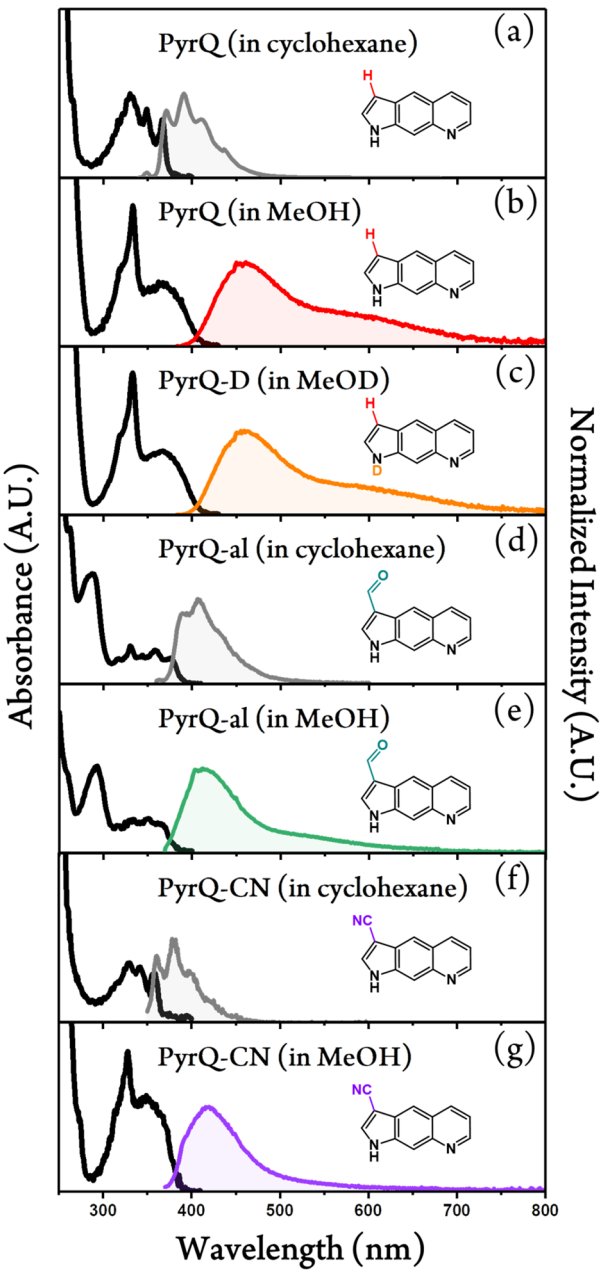

Fig. 2 Steady-state absorption (black solid lines) and photoluminescence spectra of (a) **PyrQ** in cyclohexane, (b) **PyrQ** in methanol, (c) **PyrQ-D** in methanol-OD, (d) **PyrQ-al** in cyclohexane, (e) **PyrQ-CN** in methanol, (f) **PyrQ-CN** in cyclohexane, and (g) **PyrQ-CN** in methanol at room temperature. For the emission, the excitation wavelength λ_{ex} is at their $S_0 \rightarrow S_1$ absorption peak. Also, A.U. in the *y*-axis denotes the arbitrary unit.

ground state, most plausibly using the pyridinyl N(8) site and the pyrrolic N(1)–H proton of **PyrQs** as the proton acceptor and donor, respectively.[22] This viewpoint is further supported by the following emission spectra and MD approaches.

Upon excitation, **PyrQ**, **PyrQ-al**, and **PyrQ-CN** in cyclohexane exhibit a deep violet emission maximized at 392 nm, 406 nm, and 380 nm, respectively, and possess a vibronic feature that is mirror imaged with their corresponding absorption spectra. The photoluminescence quantum yield (PLQY) was measured to be 25.7%, 5.5%, and 4.2% for **PyrQ**, **PyrQ-al**, and **PyrQ-CN**, respectively (see Table 1), where a high PLQY of **PyrQ** indicates the structural rigidity of the core, and hence, low internal reorganization energy. In other polar aprotic solvents such as CH_2Cl_2, similarly, all studied **PyrQs** exhibited solely normal Stokes-shifted emission, and no anomalous emission phenomenon was observed (see Fig. S25†).

In methanol, by sharp contrast, the electronic excitation of all **PyrQs** revealed dual emission, consisting of a blue emission band maximized at 461 nm, 413 nm, and 416 nm, denoted as the F_1 band, and an obvious shoulder (the F_2 band) located at approximately 600 nm, 527 nm, and 524 nm for **PyrQ**, **PyrQ-al**, and **PyrQ-CN**, respectively. The excitation spectra monitored at the F_1 and F_2 bands are identical, and also resemble the absorption spectrum (see Fig. S23†). Therefore, the dual emission originating from the same ground state is unambiguous, and two emissions correlated with two excited states are expected to possess a precursor-successor kinetic relationship (*vide infra*).

Knowing that the dual emission properties are only observed in protic solvents when the H-bonding formation with **PyrQs** in the ground state has been verified (*vide supra*), it is reasonable to propose the occurrence of excited-state SCPT in methanol, where protons migrate from the N(1)–H site to the N(8) site of the amino-form (Scheme 1d) *via* a solvent H-bonded relay, yielding the proton-transferred imino-form. The amino-conformer and the imino-conformer thus exhibit F_1 and F_2 bands, respectively (Scheme 1d).

To gain in-depth insight into the SCPT dynamics, we then probed the fluorescence relaxation dynamics by carrying out time-resolved fluorescence spectroscopy. Because the F_1 and F_2 bands can be resolved in a steady-state manner, we predicted the kinetics of SCPT for **PyrQs** to be relatively slow in the range of tens to hundred picoseconds. We therefore exploited the time-correlated single-photon counting (TCSPC) technique, coupled with a femtosecond Ti:sapphire laser as an excitation source (120 fs) and a fast MCP-PMT detector as the acquisition system. This overall system response time gives approximately 13 ps resolution after deconvolution.

In our experience, if the associated kinetic time constant is >15 ps, the current TCSPC system with its low excitation photon flux and rapid counting speed is more reliable than that of the femtosecond emission up-conversion technique currently used in our laboratory. Fig. 3a and b depicts the emission relaxation profiles of **PyrQs** monitored at the F_1 and F_2 bands, and their pertinent data are displayed in Table 2. For **PyrQ**, upon monitoring at the F_1 band emission of, *e.g.*, 450 nm, the relaxation of emission reveals a single exponential decay component (Fig. 3a), and the lifetime was fitted to be 44 ps.

When monitoring at the F_2 band region of, *e.g.*, 640 nm, the most optimal fit for the kinetic profile is an increasing component of 42 ps and two exponential decay time constants of 45 ps and 427 ps (Fig. 3b). The 42 ps risetime component, within experimental uncertainty, is consistent with the 44 ps decay time constant for normal emission (the F_1 band). Firm support for this viewpoint is given by the deconvolution of the F_2 band (640 nm), which is composed of a rise (44 ps) and two decay (44 ps and 427 ps) components under the consideration of the system response function (see Fig. 3c).

In cyclohexane, where no SCPT takes place, the lifetime of **PyrQ**'s normal emission (the F_1 band) was measured to be as long as 3.7 ns (see Fig. S27†). Therefore, it is reasonable for us to assume that the decay of the F_1 band in methanol is dominated by the rate of SCPT. We thus concluded that the rate of SCPT (**PyrQ**) was equal to the inverse of 44 ps, which is $2.27 \times 10^{10}\ s^{-1}$. Next, the approximately 45 ps decay component monitored at 640 nm was more plausibly attributed to the residue of the F_1 emission. This viewpoint can be rationalized by minimal separation between the proximal F_1 and F_2 bands. In addition, the radiative decay rate constant for the F_1 band was significantly larger than that of the F_2 band (*vide infra*). Therefore, despite the fact that the F_1 emission intensity was rather low at 640 nm, its contribution to TCSPC is non-negligible. Finally, the 427 ps decay component of the F_2 band can reasonably be ascribed to the population decay of the imino-tautomer.

The TCSPC data for **PyrQ-al** and **PyrQ-CN** emissions are also depicted in Fig. 3a and b. The decay lifetimes of F_1 for **PyrQ-al** and **PyrQ-CN** were fitted at 100 ps and 155 ps, respectively, which correlate well with the risetime of the corresponding F_2 bands of 104 ps and 155 ps, respectively (see Table 2). The rate of SCPT (k_{SCPT}), taking the inverse of the F_1 decay time (*vide*

Table 1 The steady-state absorption and emission data and pK_a for proton-donating and -accepting sites of the studied PyrQs and N(1)-D PyrQ

		λ_{ab}[a]	λ_{em}[b]	ϕ[c]	pK_a	
Name	Solvent	nm	nm	%	N(1)-H	N(8)-H$^+$
PyrQ	C_6H_{12}	330	391	26	~14	6.3
	CH_3OH	367	461 (F_1) 600 (F_2)[d]	0.2		
PyrQ-D	CH_3OD	367	461 (F_1) 600 (F_2)[d]	0.4	—	—
PyrQ-al	C_6H_{12}	331	406	5.5	11.8	5.3
	CH_3OH	351	413 ~527[d]	1.0		
PyrQ-CN	C_6H_{12}	327	382	4.2	11.6	5.1
	CH_3OH	349	416 (F_1)[d] ~524 (F_2)[d]	1.1		

[a] The absorption peak wavelength in cyclohexane or methanol. [b] The fluorescence peak wavelength in cyclohexane or methanol. The excitation wavelength was selected at the $S_0 \rightarrow S_1$ absorption peak wavelength for all studied compounds. [c] The photoluminescence quantum yield of all titled compounds in cyclohexane or methanol, which was calculated by comparing with the quantum yield of 87% for Coumarin 480 (in methanol).[28] [d] The appearance of a shoulder.

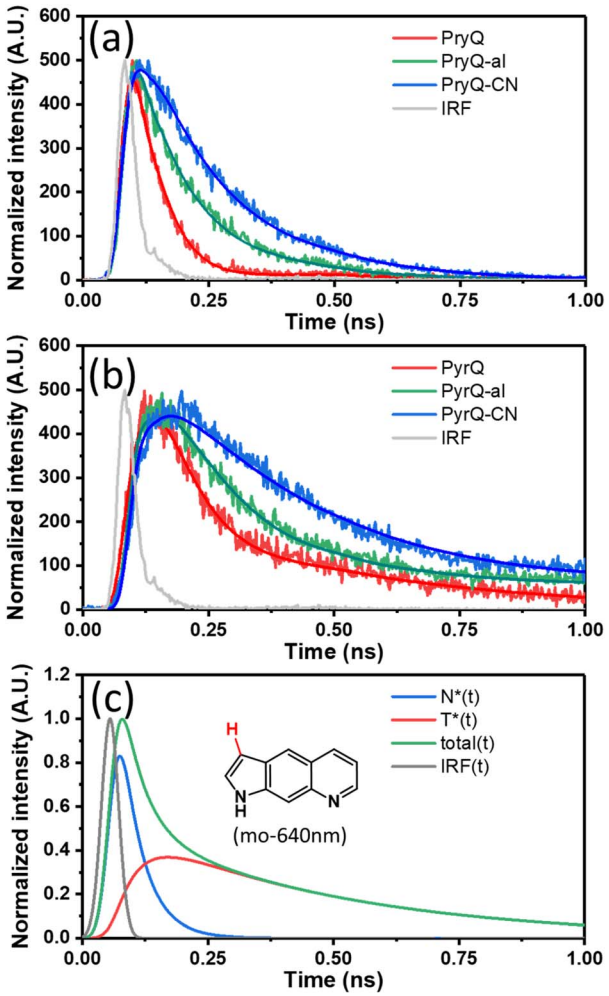

Fig. 3 The normalized time-resolved fluorescence of **PyrQ**, **PyrQ-al**, and **PyrQ-CN** in methanol monitored at the (a) F_1 and (b) F_2 bands in the region of <1 ns where the rise component of the F_2 band can be clearly observed. (c) The deconvolution of relaxation kinetics of the F_2 emission for **PyrQ** in MeOH is shown (monitored at 640 nm), which clearly indicates the cancellation of the decay and rise features due to the non-negligible overlap between normal and tautomer emissions. The simulation includes the system response function.

supra), is in the order of **PyrQ** (2.27×10^{10} s^{-1}) > **PyrQ-al** (1.00×10^{10} s^{-1}) > **PyrQ-CN** (0.65×10^{10} s^{-1}). These results imply that an increase in the electron-withdrawing ability at the C(3)-position decreases the rate of SCPT, which seems to be contradictory to the expected increase in k_{SCPT} due to the increase in the N(1)–H acidity by the C(3) electron-withdrawing strength *via* a resonance effect. This puzzle is reminiscent of previously reported SCPT molecules where the chemical substitution not only influenced the proton-donating site but also the proton-accepting site.[14–22]

Table 2 Time-resolved fluorescence of **PyrQs** in methanol and **PyrQ-D** in methanol-d (O-D) monitored at the difference emission wavelength[a]

	F_1 band		F_2 band			
Compound	λ_{em} (nm)	τ_{decay} (ps)	λ_{em} (nm)	τ_{decay1} (ps)	τ_{rise} (ps)	τ_{decay2} (ps)
PyrQ	450	44	640	45	42	427
PyrQ-D	450	74	640	76	78	834
PyrQ-al	395	100	550	105	104	3262
PyrQ-CN	420	155	600	157	155	2922

[a] The excitation wavelength was selected at the S_0 to S_1 absorption peak for all studied compounds.

To probe the interplay between the proton-donating and -accepting sites of **PyrQs**, pK_a values for the pyrrolic proton N(1)–H and the protonated pyridium N(8)$^+$–H in **PyrQs** were measured by pH-titration absorption spectrometry in water. The titration spectra are shown in Fig. S29,† and the pertinent data are listed in Table 1. As a result, the pK_a value of the N(1)–H proton was measured to be **PyrQ** (approximately 14), **PyrQ-al** (11.8), and **PyrQ-CN** (11.6) at room temperature, and decreased upon increase in the electron-withdrawing ability from H in the aldehyde to the cyano group. In yet another approach, the pK_a of the N(8)$^+$–H proton at 25 °C was also measured by absorption pH titration and determined to be 6.3, 5.3, and 5.1 for **PyrQ**, **PyrQ-al**, and **PyrQ-CN**, respectively. Accordingly, the pK_b of the N(8) site, based on pK_a + pK_b = 14, was calculated to be 7.7, 8.7, and 8.9 for **PyrQ**, **PyrQ-al**, and **PyrQ-CN**, respectively. Therefore, the basicity is in the order of **PyrQ** > **PyrQ-al** > **PyrQ-CN**. In other words, the N(1)–H donor and N(8) proton acceptor are influenced by the C(3) substitution *via* a resonance effect.

It should be noted that we are aware that excited-state phenomena would be based on excited-state pK_a^* values (* denotes the electronically excited state), which are conventionally measured by fluorescence pH titration experiments. However, the validity of this approach is based on the establishment of excited-state equilibrium between the protonated and deprotonated species, which is not the case due to the fast SCPT of tens to hundred ps for the studied **PyrQs**. Therefore, we only acquired the pK_a for each site and assumed a similar trend for pK_a^* in the excited state.

Fig. 4 depicts a plot of the rate constant for excited-state SCPT (k_{SCPT}) as a function of the pK_b of the N(8) site. The trend of increasing k_{SCPT} upon increase in the N(8) basicity infers that the rate-determining step is prone to the proton-accepting property of the N(8) site rather than the proton donation of the N(1)–H site. Further in-depth discussion will be elaborated in the section on MD simulation.[29]

We also performed time-resolved fluorescence measurement of N(1)–H-deuterated **PyrQ**, namely **PyrQ-D** in methanol-d_1 (CH_3OD). The observed k_{SCPT} rate and the tautomer population decay lifetime were 1.35×10^{10} s^{-1} (74 ps) and 834 ps, respectively. The k_{SCPT} of **PyrQ-D** was smaller than that (2.27×10^{10} s^{-1}) of **PyrQ-D** by 1.68 times. Because k_{SCPT} is the dominant decay process for the F_1 band (*vide supra*), the F_2/F_1 ratio for **PyrQ-D** is expected to be smaller than that for **PyrQ** by approximately 1.68 fold. However, as shown in Fig. 2, the 1.11 ratio of steady-state emission intensity for F_2/F_1 between **PyrQ** and **PyrQ-D** seems to conflict with the kinetic measurement (Tables 2 and S4†).

This controversy is not unusual, and can be rationalized by the different nonradiative decay rate of the F_2 band between **PyrQ** (in CH_3OH) and **PyrQ-D** (in CH_3OD). The overall PLQY was

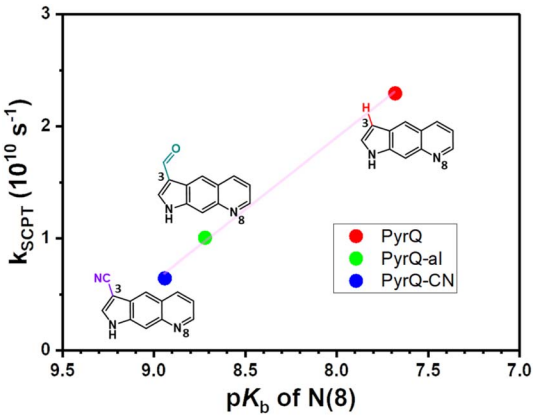

Fig. 4 A plot of the rate constants for excited-state SCPT (k_{SCPT}) of **PyrQs** as a function of the pK_b of the proton-acceptor N(8) site. The rate constants were obtained by fluorescence dynamics in methanol, and pK_a values were measured through pH titration experiments (see text).

measured to be 0.2% and 0.4% for **PyrQ** and **PyrQ-D**, respectively, in CH_3OH and CH_3OD (see Table 1). The PLQY of F_2 can be further deduced by convolution of the dual fluorescence spectra, assuming a dominant SCPT in the excited state, which gives 0.042% and 0.062% for **PyrQ** and **PyrQ-D**, respectively. For the F_2 band of **PyrQ-D** in CH_3OD, the population decay time ($1/k_{obs}$) was measured to be 834 ps, which is twice as long as 427 ps for **PyrQ** in CH_3OH (Table 2).

We applied PLQY $= k_r/k_{obs} = k_r/(k_r + k_{nr})$, where k_r and k_{nr} denote the radiative decay rate and nonradiative decay rate constants for the F_2 band, respectively. k_r and k_{nr} were then deduced and are listed in Table S4.† Clearly, while k_r of the F_2 band is approximately the same between **PyrQ** and **PyrQ-D**, the k_{nr} of 1.20×10^9 s^{-1} for **PyrQ-D** in CH_3OD is nearly twice as slow as that (2.34×10^9 s^{-1}) for **PyrQ** in CH_3OH. Because the O-D stretching frequency is lower than that of O–H, it is thus reasonable to expect that the emission quenching associated with vibronic coupling in the **PyrQ-D**/CH_3OD H-bonded complex is weaker than that in the **PyrQ**/CH_3OH H-bonded complex.

Previous reports have established a mechanism for SCRT that requires a series of H-bonded solvent molecules to bridge proton donor and acceptor parts, forming a conduit for the occurrence of a relay type of proton transfer.[14–22] Due to the great separation distance of 5.136 Å between N(1) and N(8) atoms, intuitively, there will be insufficient length with two methanol molecules to construct an H-bonded relay for the SCPT reaction in **PyrQs**.

For a solvent relay consisting of a distance greater than that of two methanol molecules, the structure of the H-bonded relay to bridge the N(1)–H and N(8) sites may have multiple configurations. To extract the population of these configurations among all randomized solvated methanol molecules, we then performed MD simulation,[29] the results of which would be able to differentiate the relay states from those of the bulk states (excluding the relay states). The details of the corresponding results and discussion are elaborated below.

Computational approach

DFT calculation. Before accessing MD, the density functional theory (DFT) calculation was performed by *Gaussian 16* (ref. 30) to gain insight into the structure–thermodynamics relationship between normal and proton-transferred tautomer forms. The molecular structure in the ground state (S_0) was optimized by DFT, and the excited-state (S_1) geometries and related optical properties were computed by time-dependent density functional theory (TD-DFT) with the B3LYP hybrid function.[31–33] 6-31+G(d,p) was used as the basis set throughout the calculation.[34–37]

The calculations were carried out in methanol using a polarizable continuum model (PCM).[38] We also performed the calculation using the CAM-B3LYP/6-31+G(d,p)[33] level (see Table S6†). In comparison, the results of B3LYP/6-31+G(d,p) were closer to the experimental values from the energy point of view, such as absorption and emission. Alternatively, the structural parameters based on B3LYP/6-31+G(d,p) seemed to be more convenient for the MD approach and will be used later.

The pertinent data for DFT calculations for **PyrQs** (in methanol) are listed in Table S5.† Clearly, the calculated absorption and emission energy gaps were consistent with the experimentally observed peak wavelengths for the amino-(normal) and imino-(tautomer) forms. For the normal form, the calculated emission gap was in the order of **PyrQ** < **PyrQ-al** < **PyrQ-CN**, which can be rationalized by the electron-withdrawing strength of the substituent at the C(3) position, which was in the order of H (**PyrQ**) < HC═O (**PyrQ-al**) < CN (**PyrQ-CN**).

As shown in Fig. 5a (also in Fig. S31 and S32†) the electron density distribution for the highest occupied molecular orbital (HOMO) for **PyrQs** covered the C(3) substituents, while it was negligible for the lowest unoccupied molecular orbital (LUMO). Therefore, the increase in electron-withdrawing strength of the C(3)-substituent decreases the energy of HOMO, whereas there is little change in LUMO (see Fig. 5a and S30–S32†), resulting in an increase in the energy gap. There is a similar argument for the tautomer form (see Fig. 5a and S30–S32†), and the calculated results were consistent with the experimental observations (Fig. 2). Fig. 5b depicts the relative energies between the normal and tautomer forms in the S_0 and S_1 states, where SCPT in the excited state is energetically favorable by >15 kcal $mole^{-1}$ for all **PyrQs**, while clearly the proton transfer is thermally unfavorable by more than 8 kcal mol^{-1} in the ground state.

We next performed preliminary DFT calculations to examine the methanol molecules required for forming the H-bonded relay suitable for SCPT of **PyrQs**. We started from two methanol molecules placed around the N(1)–H and N(8) sites of **PyrQs**, and then completed the structural optimization (Fig. 5c, d, and S33†) under a continuum model (methanol). As a result, the two methanol molecules in the methanol-**PyrQs** (2 : 1) hydrogen-bonded complex, where each methanol attaches to either the N(1)–H or N(8) site, are separated far away by >5 Å (see Fig. 5c). When three methanol molecules were used, the associated methanol-**PyrQs** complex will not be able to form a hydrogen-bonded relay configuration (Fig. 5d). After obtaining these results, we next performed the MD calculation elaborated in the following section.

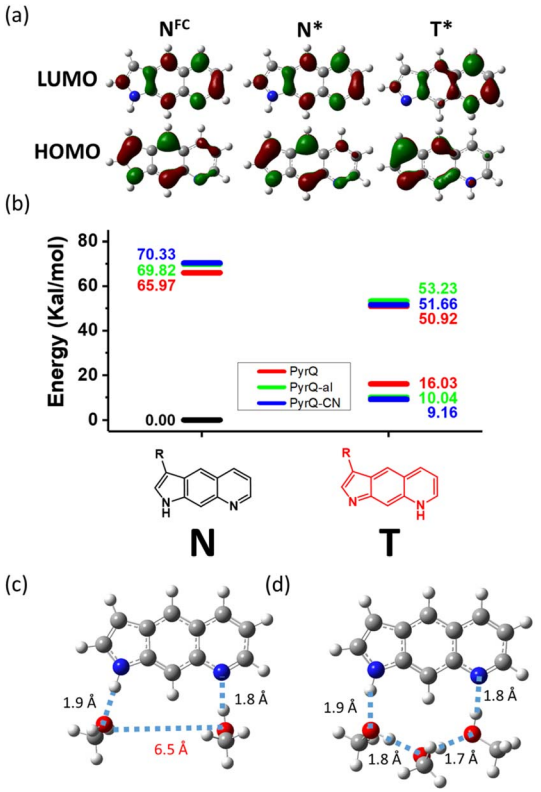

Fig. 5 (a) The electron density distribution of HOMO and LUMO for **PyrQ** monitored at Franck–Condon excitation (N^{FC}), with structural optimization at the normal S_1 (**N***) and tautomer S_1 (**T***) state. The molecular orbital isovalue was set at 0.05. See also Fig. S31 and S32† for **PyrQ-al** and **PyrQ-CN**, respectively. (b) The relative energies between the normal and tautomer forms in the S_0 and S_1 states for **PyrQs**, calculated under the methanol continuum model. (c) Upon optimization *via* the B3LYP/6–31+G(d,p) level, two methanol molecules are insufficient to form a relay to link proton-donating and -accepting sites (S_0 state). (d) Three methanol molecules linked *via* hydrogen bonds offer a reasonable relay for proton transfer from the N(1)–H to the N(8) site (S_0 state).

Molecular dynamics simulation. Herein, explicit solvent MD[29] simulations with AMBER 20 [39] were performed on a series of **PyrQ**-derived molecules (**PyrQ**, **PyrQ-D**, **PyrQ-al**, and **PyrQ-CN**) in methanol to investigate their dynamics and equilibrium between the bulk and relay state (see Fig. 6a) in methanol. The results indicate that the **PyrQs** are dynamically coupled to the methanol relay configuration in a hydrogen-bonding network (Fig. 6).

These results, together with the close-up inspections of the H-bonding configurations for each **PyrQs** in methanol, elicit two important remarks. First, methanol micro-solvation with hydrogen-bonding does exist for the N(1)–H and N(8) site in **PyrQs** (Fig. 6a). Second, there are clearly time-dependent configuration changes in the methanol relay state and bulk state (Fig. 6b). When compared with explicit methanol MD simulations, a locally fluctuating density profile is revealed, and therefore, it seems apparent that fewer trapped methanol molecules associate with the sites. Both results are consistent with the experimental observations. With MD simulation, we are able to define how many methanol molecules are feasibly required to conduct the proton transfer (Fig. 7a) and estimate the fraction of both states from the output trajectory.[40] In the current study, we used femtosecond (fs) time resolution to analyse the MD trajectory data of **PyrQs** (see the Experimental Section).

All the **PyrQ** MD trajectories were collected up to 10 ns, with every 1 fs as a snapshot resolution. The 10 ns simulated period is reasonably longer than τ_{decay} of SCPT in the current time-resolved experiment, and therefore, a total of 10^7 fs snapshot structures were used to obtain the statistics for the H-bond relay configurations. To precisely measure the time-dependent evolution of methanol relay structures in the **PyrQ:(MeOH)$_n$** complex, it is necessary for the relevant methanol orientations between N(1)–H and N(8) to strictly obey these two rules: (1) the distance between the H atom and the acceptor O or N atom (r(N–H···O) or r(O–H···O) or r(O–H···N)) must be shorter and within 2.5 Å; (2) the angle of ∠ O···H–N, ∠H–O···O, and ∠N···H–O must be 150° to 180°.

Such criteria are substantial for the complex of chains of MeOH molecules engaged in the Grotthuss-type transport[1] of a proton, *i.e.*, the proton-jump,[2] *via* an H-bond relay located between the SCPT-triggered proton donor and the proton acceptor. The relay is a group bearing an H atom able to accept an H-bond from the methanol relay group, and at the same time, form an H-bond with the proton-accepting chain. Note that because the computation time and capacity are limited, the MD simulation in the current study is based on ground-state-optimized **PyrQs**. Also, the ground-state MD simulation to probe fractions between bulk and relay configurations takes advantage of the thermally unfavorable ground-state SCPT in the relay **PyrQ** states, which eliminates the complication of simulation in the excited state due to SCPT.

The MD simulation results shown in Fig. 6 confirm the above viewpoint through observation of the transformation between the bulk state and relay state of **PyrQ**. Additionally, it was noted that the cyclic methanol train(s) is not an isolated H-bond system. There is a huge methanol source that can immediately participate in the H-bonding in the **PyrQ:(MeOH)$_n$** complex when one hydrogen bond is broken. For the observed duration up to 10 ns, the **PyrQ:(MeOH)$_n$** complexes of $n \geq 6$ were too few in fraction and can thus be ignored (Fig. 6a and 7a). These results imply that the contribution to SCPT is mainly from the configurations of **PyrQ:(MeOH)$_3$**, **PyrQ:(MeOH)$_4$**, and **PyrQ:(MeOH)$_5$**.

These results are also consistent with at least three ($n \geq 3$) methanol molecules being required to form a **PyrQ:(MeOH)$_n$** relay state in the above DFT calculation. Fig. 7a illustrates this point by showing the distributions of different cyclic relay configurations, with an equilibrium fraction less than 3%. Also, we found that the formation of 'reactive' complexing geometry requires additional nearly linear hydrogen bonds to the N(1)–H and N(8) sites, as illustrated by showing the MD snapshot of **PyrQ:(MeOH)$_3$** (Fig. S34†). Such a complex is severely inhibited in methanol solvents, whereby the fraction of **PyrQ** molecules in

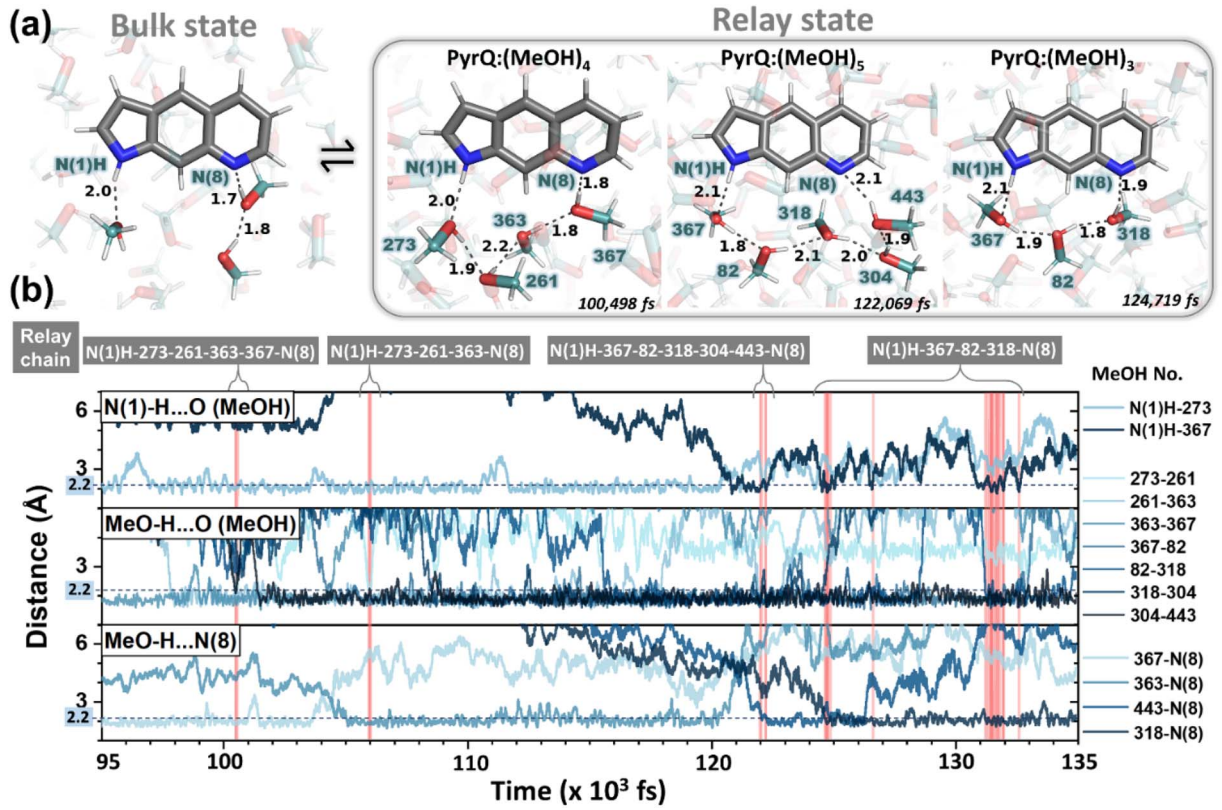

Fig. 6 Illustration of MD simulation trajectory snapshots with fs time resolution. (a) For the **PyrQ** system, in which the methanol dynamical configurations show the exchange between the bulk state and relay state. The black dotted line indicates the hydrogen bond distances between the methanol molecules (the number labelled in deep teal). (b) The time-dependent trajectory analysis of the interaction distances of **PyrQ**:(MeOH)$_n$ complexes between the relevant methanol H-bond network from **PyrQ** N(1)–H to the N(8) site, as revealed by the red highlight of different methanol relay chains appearing in time evolution.

'reactive' states is observed to be less than 1%. Thus, it can be rationalized that the small proportion of reactive solvation states is due to geometry.[40]

From the view of MD fs dynamics (see Fig. 6 and Movie S1†), the hydrogen-bonding network is switched to different relay states by the rapid rotation of the methanol OH group, which

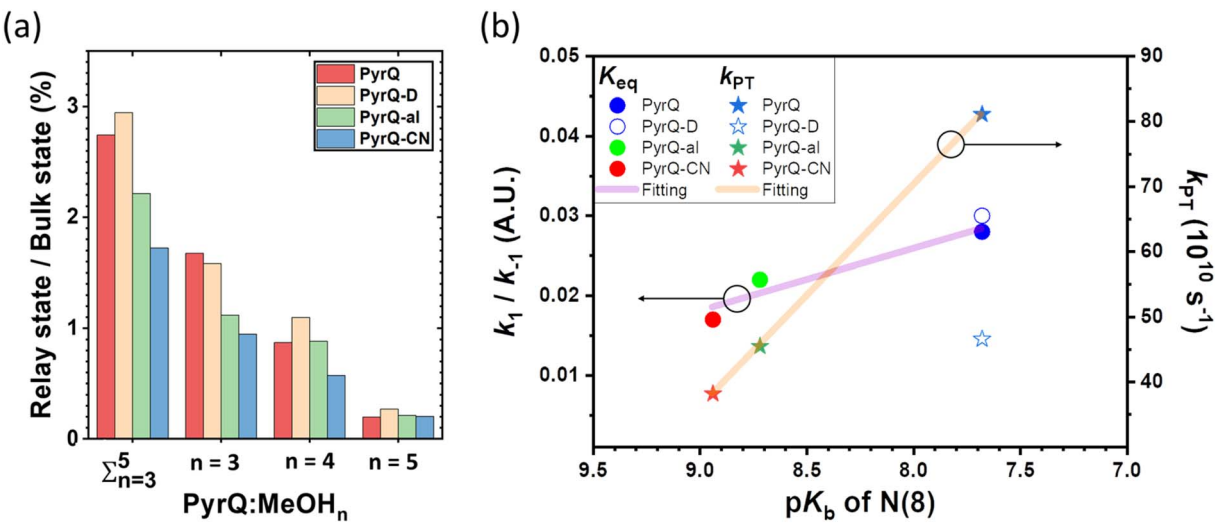

Fig. 7 (a) The 10 ns MD trajectory statistics (with 10^7 fs configurations) of the **PyrQs**:(MeOH)$_n$ complex population in the different relay chain structures and their ratio *versus* the bulk states. (b) The plot shows the equilibrium constant (K_{eq}) and the proton transfer rate (k_{PT}) *versus* the N(8) site pK_b. The left and right *y*-axes are the K_{eq} and k_{PT}, respectively. The purple and orange solid lines were obtained by fitting **PyrQ**, **PyrQ-al**, and **PyrQ-CN** using a linear relationship. Note that the deuterium isotope significantly affects k_{PT}, but K_{eq} is not significant. It is assumed that the N(8) pK_b for **PyrQ-D** and **PyrQ** are the same.

thus facilitates the reorganization of the intermolecular H-bond network as well as the exchange of the surrounding MeOH molecules, and therefore converts **PyrQs** to the bulk state.

As shown in Fig. 7a, we can easily and clearly determine the continuum relay state and the bulk state and consider the fluctuation in the femtosecond scale. To consider $n = 3$, 4, and 5 for **PyrQs:(MeOH)$_n$**, the bulk state existence time (τ_1) and the relay state existence time (τ_{-1}) were counted within an observed duration of 10 ns (see Fig. 7a). In concept, this existence time (τ_1 and τ_{-1}) was analyzed by the MD trajectory statistics, and τ_{-1}/τ_1 thus is equivalent to a pre-equilibrium constant K_{eq} between the bulk and relay type of solvation. If one assumes $1/\tau_{-1}$, denoted as k_{-1}, is >proton-transfer (tunneling) rate k_{PT} (see Scheme 3), the overall excited-state SCPT rate k_{SCPT} can be expressed by eqn (1) below.[40–42]

$$k_{SCPT} = \frac{\tau_{-1}}{\tau_1} \times k_{PT} = \frac{k_1}{k_{-1}} \times k_{PT} = K_{eq} \times k_{PT} \quad (1)$$

The K_{eq} value calculated by MD simulation (see Table 3) was used in eqn (1), as well as the experimentally obtained k_{SCPT} (Table 2), and thus, the proton tunnelling rate k_{PT} was calculated to be 8.11×10^{11} s^{-1}, 4.55×10^{11} s^{-1}, and 3.82×10^{11} s^{-1} for **PyrQ**, **PyrQ-al**, and **PyrQ-CN**, respectively (Fig. 7b and Table 3). Clearly, the tunnelling rate k_{PT} is influenced by the N(3)-substituent and leads to a decrease in the basicity, *i.e.*, the ability to accept protons is in the order of **PyrQ** > **PyrQ-al** > **PyrQ-CN**. Therefore, it is reasonable for us to conclude that the N(8) proton-accepting process plays a role in the rate-determining step.

Experimentally, the ratio for the measured k_{SCPT} (2.27×10^{10} s^{-1}) of **PyrQ** *versus* that (1.35×10^{10} s^{-1}) of **PyrQ-D** is 1.68. Although K_{eq} is virtually the same between **PyrQ** (0.028 in CH_3OH) and **PyrQ-D** (0.029 in CH_3OD, see Table 3) from MD simulation, the major difference lies in the deduced tunnelling rate k_{PT} of 8.11×10^{11} s^{-1} for **PyrQ** *versus* 4.66×10^{11} s^{-1} for **PyrQ-D**, *i.e.*, the deuterium isotope effect for SCPT (see Fig. 7b). Finally, it should be noted that the above K_{eq} is based on the sum of the fraction of the $n = 3$ to 5 methanol relay, assuming they all undergo a similar k_{PT}. Considering that the increasing number of solvents involved in the geometrical relay leads to a decrease in the SCPT rate,[40] $n = 3$ should be considered as the major contributor to execute excited-state SCPT. Therefore, the K_{eq} deduced here is considered as an upper limit. For example, $KK_{eq} \approx 1.6\%$ (see Fig. 7a) for **PyrQ** if we only take $n = 3$ into account for the occurrence of excited-state SCPT.

Table 3 K_{eq} calculated by the ratio for the inverse of existence time (τ^{-1}) of the relay states ($n = 3$–5) *versus* that of the bulk states (τ, see text) according to the MD simulation. k_{PT} is derived from eqn (1) for PyrQs

Name	Solvent	K_{eq} [a] —	k_{PT} [b] (s^{-1})
PyrQ	CH_3OH	2.8%	8.11×10^{11}
PyrQ-D	CH_3OD	2.9%	4.66×10^{11}
PyrQ-al	CH_3OH	2.2%	4.55×10^{11}
PyrQ-CN	CH_3OH	1.7%	3.82×10^{11}

[a] Equilibrium constant between the bulk and relay states in methanol solvents calculated by MD. [b] Rate constant of proton transfer, which was calculated by eqn (1) (k_{SCPT} was measured by time-resolved fluorescence spectroscope) (see Tables S9 and S10).

Summarizing all of the above results and discussion, the overall excited-state SCPT for **PyrQs** is depicted in Scheme 3, where an equilibrium is established between bulk solvated, *i.e.*, non-H-bonded relay **PyrQs** and H-bonded relay **PyrQs**. The contribution of the H-bonded relay **PyrQs** was small (<3%), and their direct excitation and the associated fast proton transfer was not pursued in this study. The major bulk solvated **PyrQs**, upon excitation, undergo equilibration with the H-bonded relay **PyrQs** state, from which proton transfer takes place. The overall kinetic expression is depicted by eqn (1), where the tunnelling rate k_{PT} is N(3)-substituent- as well as N(1)–H deuterium isotope-dependent.

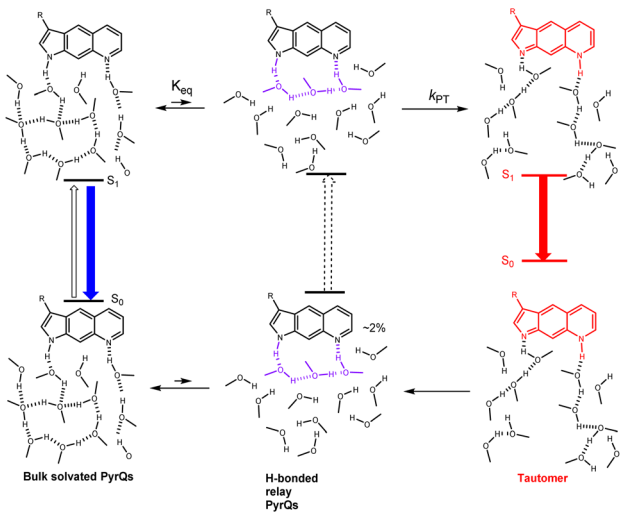

Scheme 3 The proposed overall excited-state SCPT process for PyrQs in methanol, where the H-bonded relay structure is presented using the PyrQs:(MeOH)$_3$ configuration. See the text for a detailed elaboration.

Conclusions

PyrQ and its derivatives, **PyrQ-al**, **PyrQ-CN**, were synthesized, and their physical and photophysical properties were comprehensively examined. All studied **PyrQs** underwent excited-state SCPT, in which a slower SCPT rate (k_{SCPT}) was resolved upon increasing the electron-withdrawing ability of the C(3)-substituent. MD simulation was applied to probe and analyze the solute/solvent H-bonding configuration and the solvent molecule arrangement over time for SCPT.

The statistical results confirmed that long-distance SCPT of **PyrQs** required 3–5 methanol molecules in a relay configuration to accomplish the relay-type proton transfer reaction. Further pH titration hence –N(8) basicity measurement led us to conclude that the –N(8) proton-accepting strength is the rate-determining step, which is well correlated with the intrinsic proton transfer rate k_{PT}. The overall reaction is depicted in

Scheme 3, with the associated kinetics expressed in eqn (1), where the tunnelling rate was N(3)-substituent- as well as N(1)–H deuterium isotope-dependent. The structurally rigid **PyrQs** and their sufficiently separated proton-donating and -accepting sites thus provide valuable fundamental insights into the excited-state long-range SCPT reaction.

Experimental section

General method of synthesis

All reactions were performed under nitrogen saturated. Commercially available reagents were used without drying. Chromatographic separation was carried out using silica gel from Merck (230–400 mesh). ^{1}H and ^{13}C NMR spectra were measured with a Varian Unity 400 spectrometer at 400 and 100 MHz, respectively. The chemical shifts (δ) and the coupling constants (J) were recorded in parts per million (ppm) and in Hertz (Hz), respectively.

Photophysics measurements

The absorption and emission spectra were measured by a Hitachi U-3310 spectrophotometer and Edinburgh FS980 fluorometer. Merck spectrum grade methanol used in the photophysics experiment. The pH meter (PH500 pH/mV/Temp Meter; Clean Corp.) employed an electrode of Polilyte HT (Hamilton). The sodium hydroxide was First Grade (Shimakyu).

An OB-900 lifetime spectrometer (Edinburgh) TCSPC system with an MCP-PMT was used for picosecond time-resolved measurement in these studies. The light source was femtosecond laser pulses at 740 nm (Tsunami, Spectra-Physics), and second-harmonic generation (SHG, 370 nm) of pulses was selected. The polarization of excitation was set at a magic angle (54.7°) to eliminate the anisotropy.

MD simulations on solvated PyrQ systems

To observe the balance between the bulk state and the relay state of the **PyrQs:(MeOH)$_n$** complex, we performed MD simulations with the AMBER program.[39] The partial charges of **PyrQs** and methanol molecules were calculated by DFT B3LYP/6-31G+(p,d) optimization. The Mulliken charges of atoms were added to the force field. The quantum calculations were performed in the Gaussian 16 package.[30] The initial configurations of the systems consisted of one **PyrQ** molecule and 710 methanol molecules, which were generated using the *PACKMOL package*[43] in a simulation box of 60^3 Å^3 with a density of approximately 0.4 g cm^{-3}.

All simulations began from a random configuration, energy minimization was carried out by a combination of the steepest descent and conjugated gradient method for 20 000 steps. Then, the simulation box was slowly compressed to a target density of approximately 0.8 g cm^{-3}. This simulation occurred at 300 K over 10 ns with the NVT ensemble. A constant pressure and constant temperature (NPT ensemble) simulation was performed at 300 K and 1 atm for 1 ns to allow the molecules overcome the local traped well undergoing the thermal relaxation process. Energies and densities were monitored to ensure adequate convergence within the equilibration period. After equilibration, the 10 ns NVT ensemble was implemented at 300 K to collect 10^7 fs snapshots per system for the time-resolved structural analyses.

Data availability

The photophysics spectrum, dynamic data, and MD trajectory results in this paper are available from the authors.

Author contributions

Prof. Pi-Tai Chou designed and guided all the investigations. Prof. Hsiao-Ching Yang led the theoretical study and MD simulation. Yu-Chiang Peng, Jiun-Chi Liu, Ying-Hsuan Liu, and Kai-Hsin Chang carried out the synthesis of all titled compounds. Kai-Hsin Chang and Chao-Hsien Hsu performed all the spectroscopic and dynamic measurements. Kai-Hsin Chang performed the DFT computation using the Gaussian program. Kuan-Hsuan Su and Yi-Hsien Lin performed the MD simulation using the Amber program.

Conflicts of interest

The authors declare no competing interests.

Acknowledgements

P.-T. C. and H.-C. Y. thank the National Science and Technology Council, Taiwan and Ministry of Science and Technology, Taiwan, for financial support (NSTC 111-2639-M-002-005-ASP and NSTC 111-2113-M-030-003). P.-T. C. gratefully thanks Ms Shou-Ling Huang for the assistance in NMR experiments at the Instrumentation Center at NTU, which is supported by the Ministry of Science and Technology, Taiwan. We acknowledge MOST for research support (MOST 110-2731-M-002-001, XRD000200) in performing the single-crystal X-ray diffraction measurements at the Instrumentation Center, National Taiwan University. This work was financially supported by the Ministry of Science and Technology of Taiwan (MOST 109-2113-M-143-004 and 108-2113-M-143-002). The authors thank Ms Hsiu-Ni Huang (Instrumentation Centre of National Taiwan Normal University; MS005900) for technical support.

Notes and references

1 C. J. T. de Grotthuss, *Ann. Chim.*, 1806, **58**, 54–73.
2 N. Agmon, *Chem. Phys. Lett.*, 1995, **244**, 456–462.
3 K.-D. Kreuer, *Chem. Mater.*, 1996, **8**, 610–641.
4 P. Ball, *Chem. Rev.*, 2008, **108**, 74–108.
5 S. Sharif, G. S. Denisov, M. D. Toney and H.-H. Limbach, *J. Am. Chem. Soc.*, 2006, **128**, 3375–3387.
6 M. Mohapatra and A. K. Mishra, *Photochem. Photobiol. Sci.*, 2019, **18**, 2830–2848.
7 P. K. Sengupta and M. Kasha, *Chem. Phys. Lett.*, 1979, **68**, 382–385.
8 P. T. Chou, C. Y. Wei, C. P. Chang and M. S. Kuo, *J. Phys. Chem.*, 1995, **99**, 11994–12000.

9 J. Guharay and P. K. Sengupta, *Biochem. Biophys. Res. Commun.*, 1996, **219**, 388–392.
10 V. De Filippis, S. DeBoni, E. De Dea, D. Dalzoppo, C. Grandi and A. Fontana, *Protein Sci.*, 2004, **13**, 1489–1502.
11 K. C. Ingham and M. A. El-Bayoumi, *J. Am. Chem. Soc.*, 1971, **93**, 5023.
12 C. A. Taylor, A. M. El-Bayoumi and M. Kasha, *Proc. Natl. Acad. Sci. U. S. A.*, 1969, **65**, 253.
13 K. C. Ingham and M. A. El-Bayoumi, *J. Am. Chem. Soc.*, 1974, **96**, 1674.
14 Y. Chen, R. L. Rich, F. Gai and J. W. Petrich, *J. Phys. Chem.*, 1993, **97**, 1770–1780.
15 P. T. Chou, W. S. Yu, C. Y. Wei, Y. M. Cheng and C. Y. Yang, *J. Am. Chem. Soc.*, 2001, **123**, 3599–3600.
16 J. Waluk, *Acc. Chem. Res.*, 2003, **36**, 832–838.
17 J. Waluk, S. J. Komorowski and J. Herbich, *J. Phys. Chem.*, 1986, **90**, 3868–3871.
18 J. Herbich, J. Dobkowski, R. P. Thummel, V. Hegde and J. Waluk, *J. Phys. Chem. A*, 1997, **101**, 5839–5845.
19 A. Kyrychenko, J. Herbich, M. Izydorzak, M. Gil, J. Dobkowski, F. Y. Wu, R. P. Thummel and J. Waluk, *Isr. J. Chem.*, 1999, **39**, 309–318.
20 J. Konijnenberg, G. B. Ekelmans, A. H. Huizer and C. A. G. O. Varma, *J. Chem. Soc., Faraday Trans. 2*, 1989, **85**, 39–51.
21 S. F. Mason, J. Philp and B. E. Smith, *J. Chem. Soc. A*, 1968, 3051.
22 K. H. Chang, Y. H. Liu, J. C. Liu, Y. C. Peng, Y. H. Yang, Z. B. Li, R. H. Jheng, C. M. Chao, K. M. Liu and P. T. Chou, *Chem. – Eur. J.*, 2019, **25**, 14972–14982.
23 S. M. Westaway, Y. K. Chung, J. B. Davis, V. Holland, J. C. Jerman, S. J. Medhurst, H. K. Rami, G. Stemp, A. J. Stevens, M. Thompson, K. Y. Winbornb and J. Wright, *Bioorg. Med. Chem. Lett.*, 2006, **16**, 4533–4536.
24 R. D Patil and Y. Sassona, *Org. Chem.: Curr. Res.*, 2015, **4**, 1000154.
25 K. Sonogashira, *J. Organomet. Chem.*, 2002, **653**, 46–49.
26 M. Hayashi, *Chem. Rec.*, 2008, **8**, 252–267.
27 A. Vilsmeier and A. Haack, *Ber. Dtsch. Chem. Ges. B*, 1927, **60**, 119–122.
28 A. N. Fletcher and D. E. Bliss, Laser Dye Stability. Part 5, Effect of Chemical Substituents of Bicyclic Dyes Upon Photodegradation Parameters, *Appl. Phys.*, 1978, **16**, 289–295.
29 W. F. v. Gunsteren and H. J. C. Berendsen, *Angew. Chem., Int. Ed. Engl.*, 1990, **29**, 992–1023.
30 M. J. Frisch, G. W. Trucks, H. B. Schlegel, G. E. Scuseria, M. A. Robb, J. R. Cheeseman, G. Scalmani, V. Barone, G. A. Petersson, H. Nakatsuji, X. Li, M. Caricato, A. V. Marenich, J. Bloino, B. G. Janesko, R. Gomperts, B. Mennucci, H. P. Hratchian, J. V. Ortiz, A. F. Izmaylov, J. L. Sonnenberg, D. Williams-Young, F. Ding, F. Lipparini, F. Egidi, J. Goings, B. Peng, A. Petrone, T. Henderson, D. Ranasinghe, V. G. Zakrzewski, J. Gao, N. Rega, G. Zheng, W. Liang, M. Hada, M. Ehara, K. Toyota, R. Fukuda, J. Hasegawa, M. Ishida, T. Nakajima, Y. Honda, O. Kitao, H. Nakai, T. Vreven, K. Throssell, J. A. Montgomery, Jr., J. E. Peralta, F. Ogliaro, M. J. Bearpark, J. J. Heyd, E. N. Brothers, K. N. Kudin, V. N. Staroverov, T. A. Keith, R. Kobayashi, J. Normand, K. Raghavachari, A. P. Rendell, J. C. Burant, S. S. Iyengar, J. Tomasi, M. Cossi, J. M. Millam, M. Klene, C. Adamo, R. Cammi, J. W. Ochterski, R. L. Martin, K. Morokuma, O. Farkas, J. B. Foresman, and D. J. Fox, *Gaussian 16, Revision B.01*, Gaussian, Inc., Wallingford CT, 2016.
31 A. Becke, *Phys. Rev. A*, 1988, **38**, 3098–3100.
32 C. Lee, W. Yang and R. Parr, *Phys. Rev. B*, 1988, **37**, 785–789.
33 T. Yanai, D. P. Tew and N. C. Handy, *Chem. Phys. Lett.*, 2004, **393**, 51–57.
34 R. Ditchfield, W. J. Hehre and J. A. Pople, *J. Chem. Phys.*, 1971, **54**, 724–728.
35 W. J. Hehre, R. Ditchfield and J. A. Pople, *J. Chem. Phys.*, 1972, **56**, 2257–2261.
36 P. C. Hariharan and J. A. Pople, *Theor. Chim. Acta*, 1973, **28**, 213–222.
37 T. Clark, J. Chandrasekhar, G. W. Spitznagel and P. v. R. Schleyer, *J. Comput. Chem.*, 1983, **4**, 294–301.
38 S. Miertuš, E. Scrocco and J. Tomasi, *J. Chem. Phys.*, 1981, **55**, 117–129.
39 D. A. Case, K. Belfon, I. Y. Ben-Shalom, S. R. Brozell, D. S. Cerutti, T. E. Cheatham, III, V. W. D. Cruzeiro, T. A. Darden, R. E. Duke, G. Giambasu, M. K. Gilson, H. Gohlke, A. W. Goetz,R. Harris, S. Izadi, S. A. Izmailov, K. Kasavajhala, A. Kovalenko, R. Krasny, T. Kurtzman, T. S. Lee, S. LeGrand, P. Li, C. Lin, J. Liu, T. Luchko, R. Luo, V. Man, K. M. Merz, Y. Miao, O. Mikhailovskii, G. Monard, H. Nguyen, A. Onufriev, F. Pan, S. Pantano, R. Qi, D. R. Roe, A. Roitberg, C. Sagui, S. Schott-Verdugo, J. Shen, C. L. Simmerling, N. R. Skrynnikov, J. Smith, J. Swails, R. C. Walker, J. Wang, L. Wilson, R. M. Wolf, X. Wu, Y. Xiong, Y. Xue, D. M. York and P. A. Kollman, *AMBER 2020*, University of California, San Francisco. 2020.
40 S. Mente and M. Maroncelli, *J. Phys. Chem. A*, 1998, **102**, 3860–3876.
41 R. S. Moog, *J. Phys. Chem.*, 1991, **95**, 10359–10369.
42 C.-C. Hsieh, K.-Y. Chen, W.-T. Hsieh, C.-H. Lai, J.-Y. Shen, C.-M. Jiang, H.-S. Duan and P.-T. Chou, *Chemphyschem*, 2008, **9**, 2221–2229.
43 L. Martínez, R. Andrade, E. G. Birgin and J. M. Martínez, *J. Comput. Chem.*, 2009, **30**, 2157–2164.